Geological Quarterly, 2024, 68: 20
DOI: http://dx.doi.org/10.7306/gq.1748

Fluid and solid inclusions in large halite veins in the Kłodawa Salt Dome (Central Poland) – insights into its development

Tomasz TOBOŁA[1, *]

[1] AGH University of Science and Technology, Faculty of Geology, Geophysics and Environmental Protection, al. A. Mickiewicza 30, 30-059 Kraków, Poland; ORCID: 0000-0002-6513-729X

Toboła, T., 2024. Fluid and solid inclusions in large halite veins in the Kłodawa Salt Dome (Central Poland) – insights into its development. Geological Quarterly, 2024, 68: 20; http://doi.org/10.7306/gq.1748

Secondary rocks are often found in salt domes. Among these, large halite crystal (LHC) veins and nests are common, as in the Kłodawa Salt Dome of Poland. Mineralogical tests carried out on LHC here showed the presence of fluid and solid inclusions in the halite crystals. The halite itself commonly exhibits birefringence, suggesting lattice stresses. Among the solid inclusions, anhydrite is the most common. Three types of anhydrite crystals have been distinguished as regards their size and occurrence, while small, rounded inclusions of sylvite appear much less frequently. Fluid inclusions are generally rare and mostly of the secondary type. This type of fluid inclusion assemblage (FIA) comprises various kinds as regards their size and shape, as well as in their liquid-to-gas phase ratio. Primary FIAs are of two types: small, chevron-like inclusions containing sylvite daughter minerals, and large liquid-gas inclusions with carnallite and other daughter minerals. The melting temperature of sylvite ranged from 90 to 278°C, and for carnallite from 68 to 142°C. Complete homogenization of the inclusions took place at temperatures between 260 and 471.2°C. This indicates the high-temperature origin of the LHC and the presence of significant amounts of K^{+}, Mg^{+2}, Ca^{+2}, and SO_4^{-2} ions in the solutions.

Key words: salt domes, anhydrite, epigenetic salt, large halite veins, hydrothermal environment.

INTRODUCTION

The development of salt domes is one of the most interesting geological processes, to which many field observations and geophysical analyses have been devoted (e.g., Trusheim, 1960; Talbot and Jackson, 1987; Talbot, 1993; Koyi, 1998). Large-scale salt movements are related to two main forces:

- halokinesis, defined as "a collective term for all processes connected causally with the autonomous, isostatic movement of salt" (Trusheim, 1960);
- halotectonic, in which compressive tectonic forces cause the movement of salt.

These two forces play very different roles in the development of individual salt domes. Both are associated with petrological and mineralogical changes within salt formations caused by pressure, elevated temperature, and the movement of salt masses. These changes result from the physical and mechanical properties of evaporite minerals.

Generally, hydrated minerals such as carnallite, kieserite, epsomite, gypsum, etc., are the most susceptible to temperature and pressure changes (Borchert and Muir, 1964; Łaszkiewicz, 1967; Stańczyk, 1970; Braitsch, 1971; Stańczyk-Stasik, 1976; Sonnenfeld, 1984). The decomposition of these minerals under the influence of increasing temperature and pressure releases considerable quantities of water, which is a good polar solvent and reacts with other minerals. In contrast, minerals such as halite and sylvite are much more resistant to temperature and pressure, but a small amount of water significantly changes their properties by increasing their solubility with a rise in temperature.

The migration of a salt solution within the salt deposit causes ion exchange between the host rocks, resulting in the crystallization of epigenetic minerals. Another way to create epigenetic minerals is by changing the physical properties of the salt solution, for example, its temperature. Cooling down salt solutions often induces crystallization due to the decrease in the solubility of most chemical compounds as temperature drops.

In the Kłodawa Salt Dome (KSD), as in other salt domes in the Polish Lowland, there are various secondary epigenetic deposits. Their occurrence, form, mineral composition, and relation to the surrounding rocks have been studied by Stańczyk-Stasik (1976). This study primarily focused on sulphate salts and, to a lesser extent, on chloride salts. The presence of secondary veins and nests composed of large halite crystals (LHC) has been recorded both in salt domes (e.g., Czapowski et al., 2009) and in disturbed bedded salts (e.g., Banaszak et al., 2007; Schléder et al., 2008). Although secondary veins of LHC frequently occur in salt-bearing deposits, they have not previously been researched in detail.

LHC should be classified as part of the group of "anomalous salts" (Kupfer, 1976, 1980, 1990; Looff et al., 2010; Looff, 2017;

* E-mail: tobolatomasz@agh.edu.pl

Received: January 26, 2024; accepted: April 19, 2024; first published online: 8 July, 2024

Warren, 2017) due to their coarse-grained texture and their occurrence in the form of veins or nests. Anomalous salts are distinguished by structural and textural features, colour, impurity contents, and other petrological characteristics. They were first described by Kupfer (1990), and later by Looff et al. (2010) and Warren (2017). They form areas considered as shear zones and locations where salt leakage occurs (Warren, 2017). Due to their unusual development, they possess different geomechanical properties than the surrounding salts, and therefore, they require special attention during salt deposit exploitation (Looff et al., 2010; Looff, 2017).

The aim of this study is to attempt to determine the physicochemical conditions of LHC veins and nests formation in the KSD, constraining the physicochemical conditions of secondary halite crystallization by fluid and solid inclusion studies. The LHC veins and nests are evidently secondary formations, their origin linked to the various stages of salt dome formation. As such, they mirror parameters such as temperature, pressure, and the chemical composition of migrating brines during halotectonic or halokinetic movements. Understanding these conditions helps us discern the conditions surrounding salt dome formation.

GEOLOGICAL SETTING

The KSD is located in central Poland (Fig. 1A) and belongs to the Izbica Kujawska-Łęczyca anticlinal salt structure, which is located at the SW edge of the Mid-Polish Trough (MPT), and extends generally NW–SE. The MPT is a deep structure which evolved during Permian to Cretaceous time along the Teisseyre-Tornquist Zone. It was filled with a complete succession of

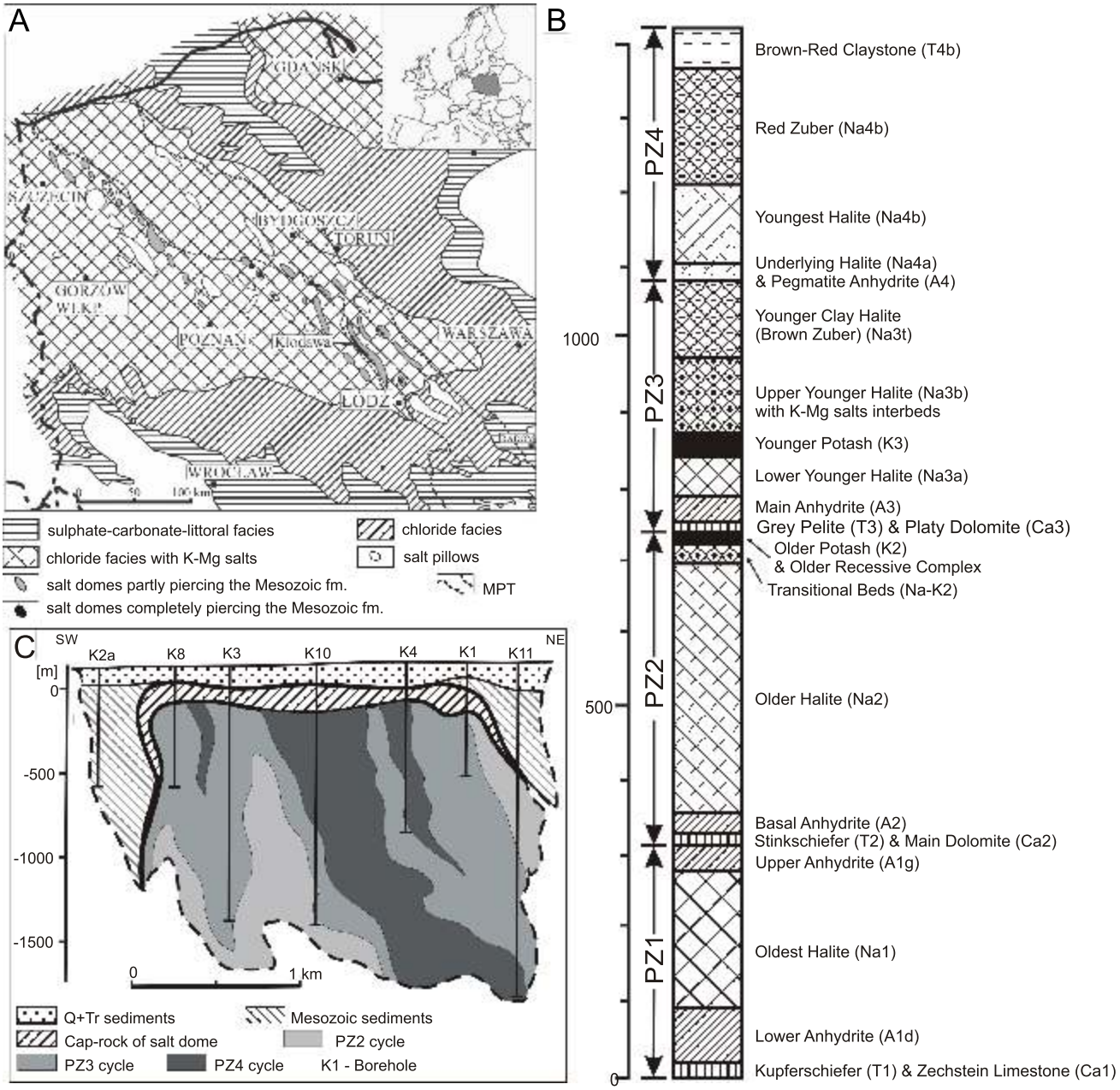

Fig. 1A – map of Zechstein lithofacies distribution in NW and central Poland with location of salt structures (after Garlicki and Szybist, 1986; MPT – Mid-Polish Trough); B – lithostratigraphic profile of the Zechstein succession in the Kłodawa salt diapir (after Garlicki and Szybist, 1991); C – geological cross-section through the upper part of the Kłodawa salt dome (after Toboła et al., 2007)

Zechstein evaporites and Mesozoic strata (Dadlez et al., 1995; Dadlez, 2003; Stephenson et al., 2003; Krzywiec, 2004b). This Zechstein evaporite succession comprises four cyclothems which are ~1500 m thick in total (Fig. 1B). Three lower cyclothems (e.g., PZ1–PZ3) are complete, classical evaporite sequences consisting of terrigenous deposits, carbonates, sulphates, rock salt and potassium-magnesium salts. Only in the uppermost part of the PZ3 cyclothem, there occurs an atypical mixture of halite and clay minerals defined as "Younger Clay Halite" (so-called Brown Zuber – Na3t; Fig. 1B). The uppermost cyclothem (PZ4) shows a terrigenous-evaporite sequence. It was subdivided into five subcyclothems (PZ4a–PZ4e) reflecting cyclic climatic changes (Wagner, 1994).

During the Late Cretaceous–Paleocene, the axial part of MPT was uplifted and significantly eroded (Dadlez et al., 1995; Wagner et al., 2002; Krzywiec et al., 2003; Krzywiec, 2004a, 2006). This development of the MPT had a considerable influence on the development of salt structures in this area.

The KSD is ~26 km long, 0.5–2 km wide and it reaches 8 km depth (Burliga et al., 1995; Schléder, et al., 2007; Wachowiak, 2010; Wachowiak and Toboła, 2014; Toboła and Wachowiak, 2018; Toboła and Botor, 2020). Its upper part is asymmetrical, with the NE side dipping moderately (55–70°) eastwards and the SW side almost vertical (Fig. 1C). The diapir is surrounded by deformed Mesozoic (Triassic–Jurassic) strata and it is overlain by Paleogene-Neogene and Quaternary deposits (Garlicki and Szybist, 2008; Toboła and Botor, 2020).

The inner structure of the KSD is complicated. The dome is built of fully developed evaporite layers which belong to the PZ2–PZ4 cyclothems. The rocks of cyclothem PZ1 are partly uncovered in the salt dome, but their stratigraphic position is uncertain (Werner et al., 1960; Kucia, 1970; Burliga et al., 1995). All these layers are strongly deformed and form a very complicated inner structure of the dome. The most frequent tectonic deformation is piercing of older by younger and youngest salt, pinching out of the layers and narrow high-amplitude folds. In the SW and NE parts of the cross-section of the diapir two main anticlines have been distinguished (Fig. 1C). These are elongated NW–SE and separated by a deep central syncline built of upper sections of the PZ3 and PZ4 cyclothems (Werner et al., 1960).

METHODS

MATERIALS

Samples of LHC were collected from the mining levels 450, 525, and 600 in the Kłodawa Salt Mine. Forty-nine samples were collected for mineralogical and fluid inclusion studies. After macroscopic observation and description, samples were selected for microscopic observation. These were prepared by cracking along the cleavage planes of previously separated single halite monocrystals. The thickness of the slabs was ~0.5–3 mm. In the next stage, the slabs with uneven or rough surfaces were ground and polished with sandpaper.

INSTRUMENTS

Microscopic observations of thick plates in transmitted light were conducted using a *Motic BA-310Pol* polarizing microscope with 4×, 10×, 40× and 60× objectives, as well as a *Nikon Eclipse E600* microscope with 5×, 20×, 50×, and 100× long-distance objectives. An additional UV source, an outside diode lamp (365 nm), was utilized to check for the presence of hydrocarbons.

Raman analysis was performed using a *ThermoScientificTM DXR Raman Microscope* operating in confocal mode, with a 532 nm excitation line laser source (grating: 900 lines/mm, spectrograph aperture: 25 µm pinhole). The acquisition time was 30 s, and the laser power was set at 5 mW. In cases where organic matter was present, the laser power was reduced to 2 mW to prevent its destruction. An *Olympus* microscope with 100x, 50x, and 10x magnification objectives was employed to focus the laser on the samples, resulting in a laser focus diameter of ~1–2 µm. The Raman system was calibrated against the 520.4 cm^{-1} line of a Si-wafer.

The decomposition of Raman spectra of organic matter was performed using *Omnic v. 8.3 Peak Resolve* and the *Fityk 0.9.8* program (Wojdyr, 2010).

Microthermometric measurements were conducted using a *Linkam THMSG600 Geology Heating* and Freezing Stage mounted on a *Nikon Eclipse E600* microscope. The stage was calibrated using pure CO_2 synthetic inclusions (Tm = –56.6°C) and known homogenization temperatures of pure H_2O inclusions. A heating-freezing rate of 5°C/min was applied with an accuracy of 0.1°C. Individual halite plates were measured only once to avoid the effect of inclusions stretching outside the observation field of the microscope, where inclusions cannot be directly observed. Cycling was attempted in all homogenization runs to observe the proper homogenization temperatures (Goldstein and Reynolds, 1994). Attention was also paid to changes in inclusion shape (Roedder, 1984b; Vanko and Bach, 2005). If noticeable changes occurred, the measurements were interrupted.

RESULTS

MACROSCOPIC OBSERVATIONS

In the Kłodawa Salt Mine, LHC often occur in the form of veins or irregular nests. They are very common on all mining levels and are found in almost all lithological strata. Within the salt rock mass, the large halite veins and nests are distinguished by the size of the crystals, which can reach several tens of centimetres, and the lack of an ordered structure (Fig. 2A). These veins, which occur within the carbonates and sulphates, often co-occur with polyhalite (Fig. 2B). The halite crystals appear macroscopically clean and transparent (Fig. 2C). However, in some veins, there are fracture systems that most frequently run at an angle of ~50°.

MICROSCOPIC OBSERVATION

Under the transmitted light microscope, the halite crystals are transparent and clear. In rare cases, they show birefringence under crossed polars, visible as a belt-like patterns that intersect at right angles and run at an angle of 45° relative to the cleavage surface (Fig. 2D), similarly to those observed by Mendelson (1961) and Carter and Heard (1970). Mostly, it is visible as one system of parallel belts or as small, irregular areas with blurred boundaries, covering only part of the crystal.

Anhydrite is the most common impurity in the halite. In all samples analysed, anhydrite occurs in three main forms that differ in size and shape, and locally intermediate stages are observed between them. The most common form consists of large crystals, some exceeding 500 µm, with well-defined, nearly

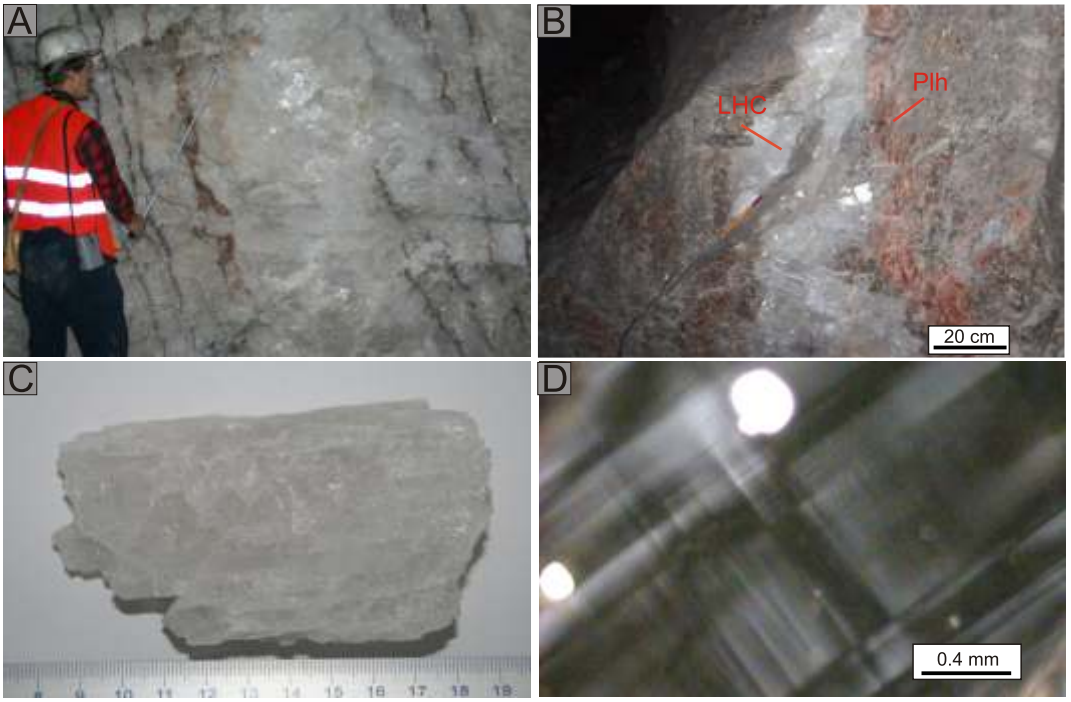

Fig. 2A – LHC veins cutting the Older Halite (Na_2); B – LHC veins with polyhalite (Plh) on the margins cutting the Main Anhydrite (A3); C – a large halite crystal with a system of cracks intersecting at an angle of ~50°; D – microscopic image of birefringence in the halite crystal

euhedral shapes (Fig. 3A). However, only their corners commonly show a slight degree of rounding. Occasionally, crystals are covered by fluid inclusions and an opaque substance, discussed below. Some of these crystals display systems of cracks filled with a brown substance (Fig. 3B). These cracks continue within the halite area over a distance of several hundred micrometres, and they are marked by groups of gas inclusions with dimensions of a few micrometres. Their course ends as a gradual reduction in the size of the inclusions until they completely disappear.

The second type of anhydrite is smaller in size (up to ~200 μm). These crystals are characterized by rounded contours, commonly almost spherical (Fig. 3C), or some are very irregularly shaped (Fig. 3D). A characteristic feature of both types of anhydrite crystal is the presence of inclusion groups on their surfaces.

The third type consists of very small anhydrite crystals whose size ranges from several tens of micrometres, rarely exceeding 50 μm (Fig. 3E). They form streaks that diagonally cross the halite crystals. They are generally oval in shape though some can be irregular. In some cases, the anhydrite streaks are accompanied by an opaque mass (Fig. 3F). In contrast to the types mentioned above, this type lacks fluid inclusions on anhydrite crystal surfaces.

The anhydrite crystals are rarely accompanied by dolomite (Fig. 4A), which was documented by Raman spectra at 176, 299, 725, 1097, 1443 cm^{-1} (Table 1). Raman spectroscopy clearly reveals that this dolomite is commonly accompanied by organic matter (OM), characterized by a Raman spectrum composed of two regions. The first, at 1000–1800 cm^{-1}, is more intensive, and the second, at 2500–3100 cm^{-1}, is weaker (Wopenka and Pasteris, 1993; Beyssac et al., 2002, 2003, 2004; Aoya et al., 2010; Lahfid et al., 2010; Lünsdorf et al., 2013; Kouketsu et al., 2014; Lünsdorf, 2016; Lünsdorf and Lünsdorf, 2016). OM locally also appears on anhydrite crystal surfaces (Fig. 4B). In all cases, the Raman spectra of the OM show similar shapes in the first region (Fig. 5A). This distribution indicates a low degree of thermal transformation (Kouketsu et al., 2014). Decomposition according to the method proposed by Kouketsu et al. (2014) revealed temperatures in the range of 110–193°C (Table 2).

In addition, oval, isotropic solid inclusions with a refractive index lower than that of halite also occur in the halite crystals (Fig. 5B). They are ~0.1 mm in size and often contain small gas bubbles on their surfaces. Raman spectra show only one peak in the low range, i.e., 199 cm^{-1}, which indicates the presence of sylvite (Krantz and Luty, 1985; Wesełucha-Birczyńska et al., 2008).

PETROGRAPHY OF FLUID INCLUSIONS IN LHC

Fluid inclusion assemblages (FIAs) are relatively rare in the LHC. Two main types of FIA can be distinguished, depending on their relationships to crystallographic axes and mode of occurrence: secondary (or pseudosecondary) and primary (Roedder, 1984a; Goldstein and Reynolds, 1994; Goldstein, 2001, 2003). The secondary FIAs predominate in most samples analysed. This type of FIA consists of various kinds of inclusion, varying in size, shape, and liquid-to-gas phase ratio. Most commonly, they form cubic or slightly elongated inclusions (Fig. 6A). The size of inclusions ranges from a few micrometres to >50 μm. Larger inclusions are filled with a variable gas-to-liquid ratio. Typically, smaller inclusions show larger gas-to-liquid ratio. In such FIAs, the linear course often coincides with the cleavage surfaces. In some cases, their course gradually disappears due to a reduction in the size of inclusions. At these end parts, the FIA course is undulating (Fig. 6B). In most FIAs, Raman spectroscopy showed no gases except for water vapour. In a few FIAs, the presence of methane, which is char-

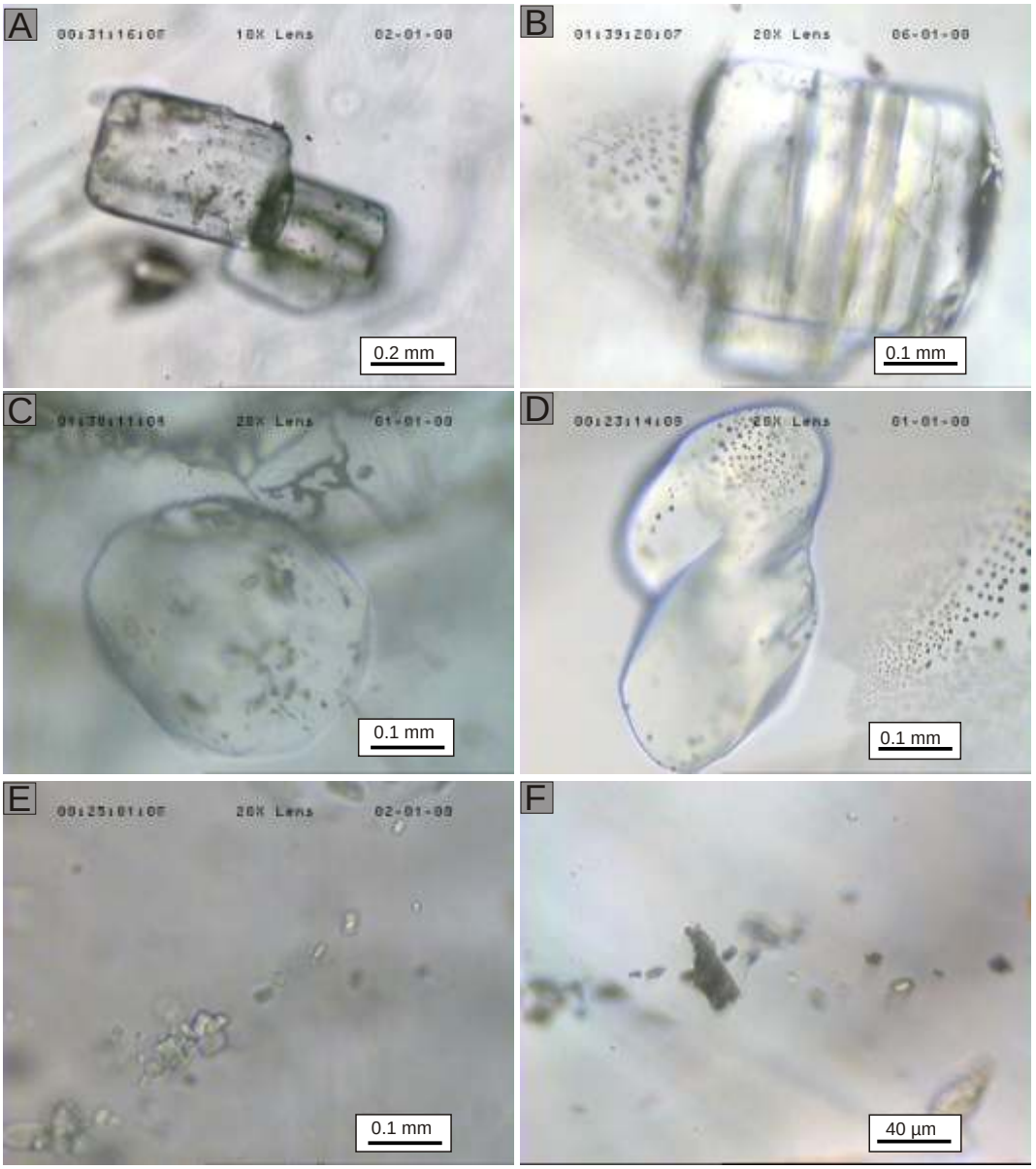

Fig. 3A – large anhydrite crystals of euhedral shape (the first type); B – the same type of anhydrite crystal as in part A with cracks filled with a brown mass; C – the second type of anhydrite crystal, of rounded shape; D – an irregularly shaped anhydrite crystal of the second type; E – very small anhydrite crystals of the third type; F – opaque contaminants in the third anhydrite type as streaks

acterized by Raman bands at 2917 cm^{-1}, has been identified (Burke, 2001).

Another type of secondary FIA is composed of larger, tubular, or slightly flattened inclusions, connected to each other in the form of a net (Fig. 6C). These FIAs transform into separated inclusions with irregular shapes, some of which contain daughter birefringent minerals (Fig. 6D).

Remarkably flattened and large fluid inclusions occur on the cleavage planes (Fig. 6E, F). They are frequent but challenging to observe under a microscope in plane polarised light due to their low thickness. They have irregular shapes with mostly wavy boundaries. Commonly, under crossed polars, large birefringent minerals are visible within the inclusions (Fig. 6F). The interference colours in the samples vary from very bright colours (second order) to first-order grey. Raman spectroscopy reveals the characteristic set of peaks for carnallite (Table 1). By considering interference colours and the optical properties of carnallite, the approximate thickness of the inclusions can be estimated using the Michel Lévy chart. In the samples studied, this thickness ranges from ~5 to 10 µm due to the grey to bright interference colours of carnallite.

Two types of primary FIA have been distinguished based on their distribution and manner of occurrence. The first type is very rare and was found in only two samples. These inclusions are liquid-solid, and their size ranges from a few to ~20 µm (Fig. 7A). In comparison to the typical primary FIAs that form chevron or hopper structures in sedimentary halite (Holdoway, 1973; Roedder, 1984b; Kovalevich et al., 1997; Galamay et al., 2019), they are less densely packed and appear larger. Furthermore, they contain cubic optically anisotropic daughter minerals. The size of these daughter minerals is proportional to the volume of the inclusions. Microscopic observations, supported by Raman analysis, indicates the presence of sylvite.

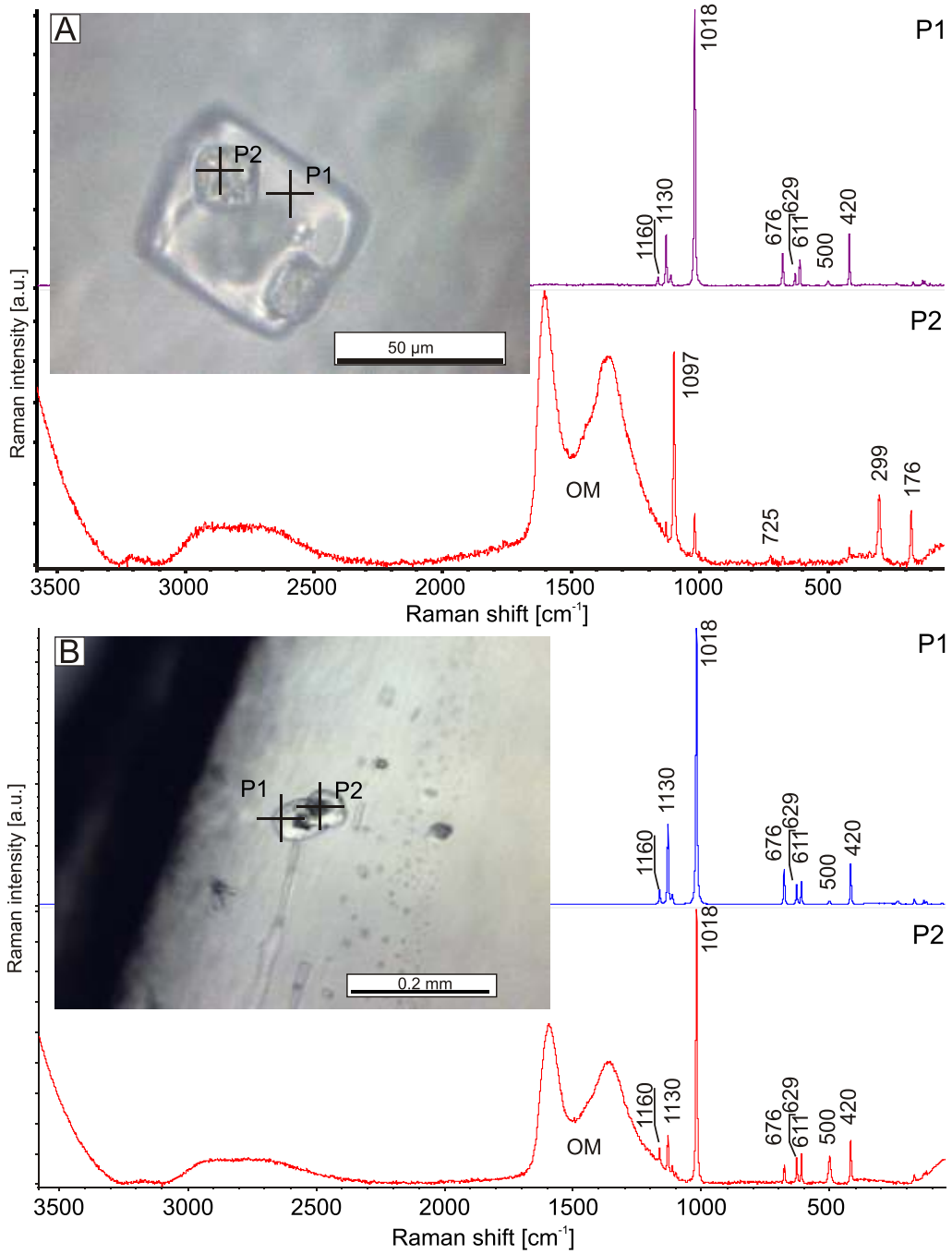

Fig. 4A – Raman spectra at points P1 (anhydrite) and P2 (dolomite with OM) and a microscopic image in reflected light of an anhydrite euhedral crystal with two small dolomite crystals accompanied by OM; B – Raman spectra and microscopic image of anhydrite with low concentrations of OM

The second type of FIA is more frequent and diverse in terms of inclusion composition. It is composed of large inclusions, reaching up to ~2 mm. These inclusions are widely spaced, as shown in Figure 7B, in contrast to the first type. They can also form groups of several inclusions or occur as separate inclusions within the halite crystals. In this type of FIA, inclusions exist in two phases: liquid–gas (LG) or liquid–solid (LS) or solid–gas (SG); or in three phases: liquid–gas–solid (LGS). The SG inclusions are difficult to distinguish from LG inclusions microscopically but can be clearly differentiated in microthermometric measurement. The LG inclusions usually have a large gas bubble occupying ~30% of the inclusion volume (Fig. 7C). The daughter minerals in LS, SG and LGS inclusions are sylvite and carnallite. Sylvite is less common than carnallite and occurs as small crystals (Fig. 7D). Carnallite is clearly visible microscopically due to its high birefringence (Fig. 8A) and has been confirmed by a characteristic set of peaks (Table 1) in Raman spectroscopy. The ratio of carnallite volume to the inclusion volume varies from ~20 to ~80%. Locally, carnallite is accompanied by small crystals of epsomite, which are not visible in mi-

Table 1

Daughter minerals found in inclusions with their diagnostic Raman bands

Mineral	Raman bands [cm^{-1}]	References
Carnallite	100, 120, 202, 657, 1645, 3247, 3433	Weber et al. (2017, 2018)
Dolomite	176, 299, 725, 1097, 1443	Frezzotti et al. (2012)
Epsomite	369, 447, 612, 984, 1095, 1672, 3303	Wang et al. (2006)
Görgeyite	281, 433, 440, 457, 480, 595, 602, 631, 654, 661, 711, 1005, 1013, 1085, 1115, 1137, 1161, 1164, 1175,1187,1215, 3525, 3579	Kloprogge et al. (2004)
Polyhalite	436, 448, 464, 477, 620, 626, 641, 652, 987 991, 1014, 1069, 1094, 1130, 1144, 1165, 1181, 3288, 3437	Wollmann et al. (2008), Jentzsch et al. (2012), Cheng et al. (2019)
Sylvite	199	Krantz and Luty (1985), Wesełucha-Birczyńska et al. (2008)

Underlined peak values are the main Raman peaks of the minerals

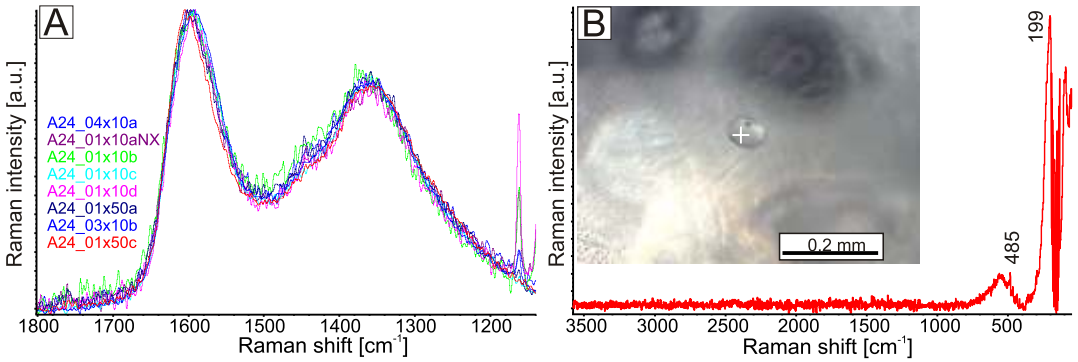

Fig. 5A – a set of Raman spectra for OM in LHC; B – Raman spectra and microscopic image of a rounded sylvite inclusion in LHC

Table 2

The main statistical parameters for homogenization temperatures obtained from microthermometric measurements and distributions of Raman spectra

	Dissolution temperature		Bulk homogenization temperature [°C]	Temperature from OM decomposition [°C]
	Sylvite [°C]	Carnallite [°C]		
Min	90.6	68.1	223.4	110.2
Max	278.0	142.0	471.2	193.0
Aver.	142.0	102.0	324.4	159.6
SD	49.9	24.3	73.6	32.2
CV [%]	35.1	23.8	22.7	20.2

SD – standard deviation, CV – variation coefficient

croscopic observation but show additional very weak peaks at 369, 447, 612 cm^{-1} and a strong peak at 984 cm^{-1} in Raman spectroscopy (Table 1). Furthermore, carnallite is accompanied by polyhalite. Polyhalite is also difficult to distinguish microscopically due to its small size but can be easily identified in Raman spectroscopy by its two characteristic peaks at 991 and 1017 cm^{-1}, among others (Table 1). Görgeyite is very rarely found as very small (a few microns) daughter minerals accompanying sylvite in fluid inclusions (Fig. 8B).

Single inclusions (Fig. 9A) occur very rarely in the samples analysed. They have a spherical shape and are ~100 μm in diameter. Raman spectroscopy reveals the presence of N_2 and H_2S gases at 2331 and 2611 cm^{-1}, respectively (Burke, 2001).

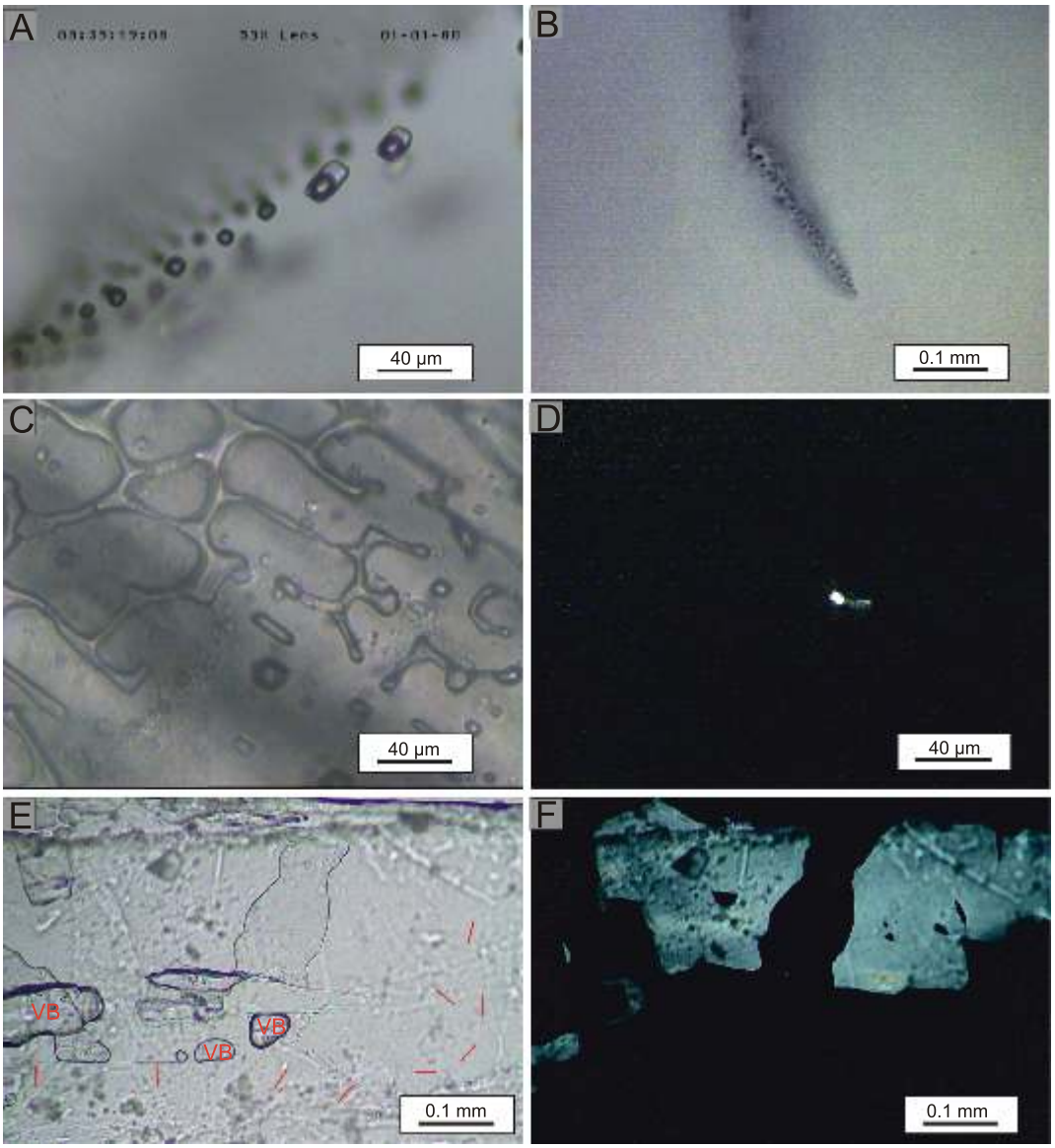

Fig. 6. Microscopic images of secondary FIAs of: A – cubic or slightly elongated inclusions; B – undulating end parts of the FIA course; C – tubular or slightly flattened FIAs; D – the same as in C in crossed polars with a small birefringent mineral visible; E, F – remarkably flattened and large fluid inclusions with vapour bubbles (VB) (arrows mark boundary of inclusion) and with a birefringent daughter mineral (E – 1N, F – XN)

MICROTHERMOMETRIC MEASURMENTS

The first type of primary FIA (Fig. 7A), characterized by sylvite as a daughter mineral, exhibited a gradual dissolution of sylvite during the heating experiments. Dissolution initiates at 36°C, with complete homogenization of sylvite observed at 90.6°C (Table 2). Continued heating led to homogenization in the subsequent inclusions, with the highest homogenization temperature recorded at 278°C. Most sylvite dissolution temperatures are <150°C (Fig. 9B), while homogenization temperatures exceeding 150°C are sporadic and characterized by a wide range of values.

The second type of primary FIA showed a greater spread of results during microthermometric experiments. In the case of inclusions containing carnallite as a daughter mineral, the initial changes occurred at low temperatures. These changes are related to the slow dissolution of carnallite. The initial point of carnallite dissolution is difficult to observe directly under the microscope due to limited visibility. Carnallite dissolves at ~1°C above room temperature. The final dissolution temperature ranges from 68.1 to 142°C (Table 2). The dissolution temperature of the carnallite daughter mineral falls within a narrower range and appears to be more homogeneous compared to the sylvite daughter mineral (Fig. 9C). Inclusions with smaller daughter minerals exhibited lower final dissolution temperatures. The final dissolution temperature increases as the ratio of daughter mineral volume to inclusion volume rises.

In inclusions where the ratio of carnallite volume to inclusion volume is small, carnallite does not immediately become evident during cooling to room temperature. Small cubic minerals, likely sylvite, occasionally appear exclusively in these inclusions. Nevertheless, carnallite re-emerges as a daughter mineral after a few days. Conversely, rapid cooling to –160°C fre-

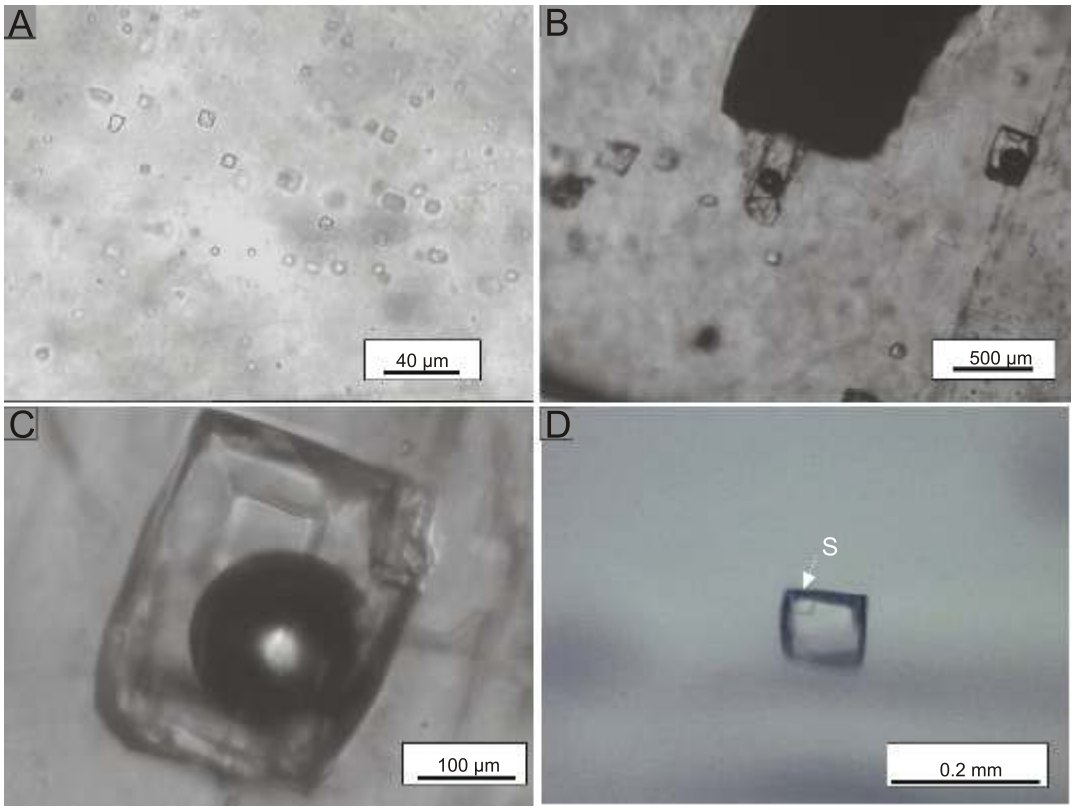

Fig. 7. Microscopic images of primary FIAs of: A – small, cubic inclusions with anisotropic daughter minerals; B – large, cuboid two-phase (LG) inclusions; C – example of a large fluid inclusion with gas a bubble occupying ~30% of the inclusion volume; D – large inclusion without gas bubble but with sylvite as daughter mineral

quently results in the appearance of a large number of small birefringent minerals (Fig. 9D).

In the secondary type of inclusions, such as those found in the flattened inclusions on the cleavage planes (Fig. 6E, F), a similar range of final dissolution for carnallite was recorded.

The low-temperature observations of inclusions with carnallite or sylvite (the second type of primary FIAs) associated with vapour bubbles (LG, SG, LGS) do not indicate the formation of ice. The only changes observed in these inclusions pertain to the size of the daughter minerals. The increase in carnallite volume was slight. In the case of inclusions with sylvite as the daughter mineral, small new crystals often appear (Fig. 9E).

Complete homogenization of inclusions was observed exclusively in the LG→L direction. The values of homogenization temperature are very high (Table 2). The homogenization temperature distribution, depicted in Figure 9F, reveals two distinct ranges: 260–350°C and 420–471.2°C. The first range was more commonly observed (Fig. 9F).

DISCUSSION

Several inferences regarding the origin of LHC veins can be derived from the results reported. The first is the birefringence of halite crystals, an exceptionally rare phenomenon that has been observed in what is commonly referred to as “blue halite” (Sonnenfeld, 1995; Heflik et al., 2008; Zelek et al., 2008, 2015; Wesełucha-Birczyńska et al., 2012), as well as in “bituminous salts” (Toboła, 2010), and in the Lotsberg Formation in Canada (Toboła and Kukiałka, 2020). It can be attributed to strain within the crystal lattice (Mendelson, 1961; Carter and Heard, 1970), as it is well known that uniaxial stress induces birefringence in optically anisotropic materials. Also in halite crystals, induced birefringence was observed at uniaxial pressures of 2.75–3.05 MPa (Cyran et al., 2023). However, this birefringence disappears once the pressure is released. In the case of LHC from the Kłodawa dome, this birefringence is permanent, indicating lasting changes in the internal structure of the crystals. These changes are related to the state of stress in the salt rock mass during the formation of LHC veins. This stress state caused the formation of cracks and allowed the migration of saline solutions.

Establishing the origin of the solutions from which significant halite crystallization occurred is essential. Within the salt deposit, several sources of free water exist. The transformation from gypsum to anhydrite has been considered (Borchert and Muir, 1964; Braitsch, 1971; Schléder et al., 2008). This transformation can occur under elevated temperatures or pressures. Borchert and Muir (1964: p. 132) reported that 1 m^3 of gypsum is transformed into 0.62 m^3 of anhydrite and 0.486 m^3 of $CaSO_4$-saturated liquid. This liquid has the capacity to dissolve halite and K-Mg minerals as it migrates through the salt rock. Another source of free water generation involves the transformation of hydrous K-Mg minerals during metamorphic processes. The most common reaction involves the decomposition of carnallite, resulting in the formation of hardsalts and the release of $MgCl_2$-saturated solutions (Borchert and Muir, 1964). Other mineral transformations, such as epsomite to kieserite, the decay of kainite, and reactions between minerals such as

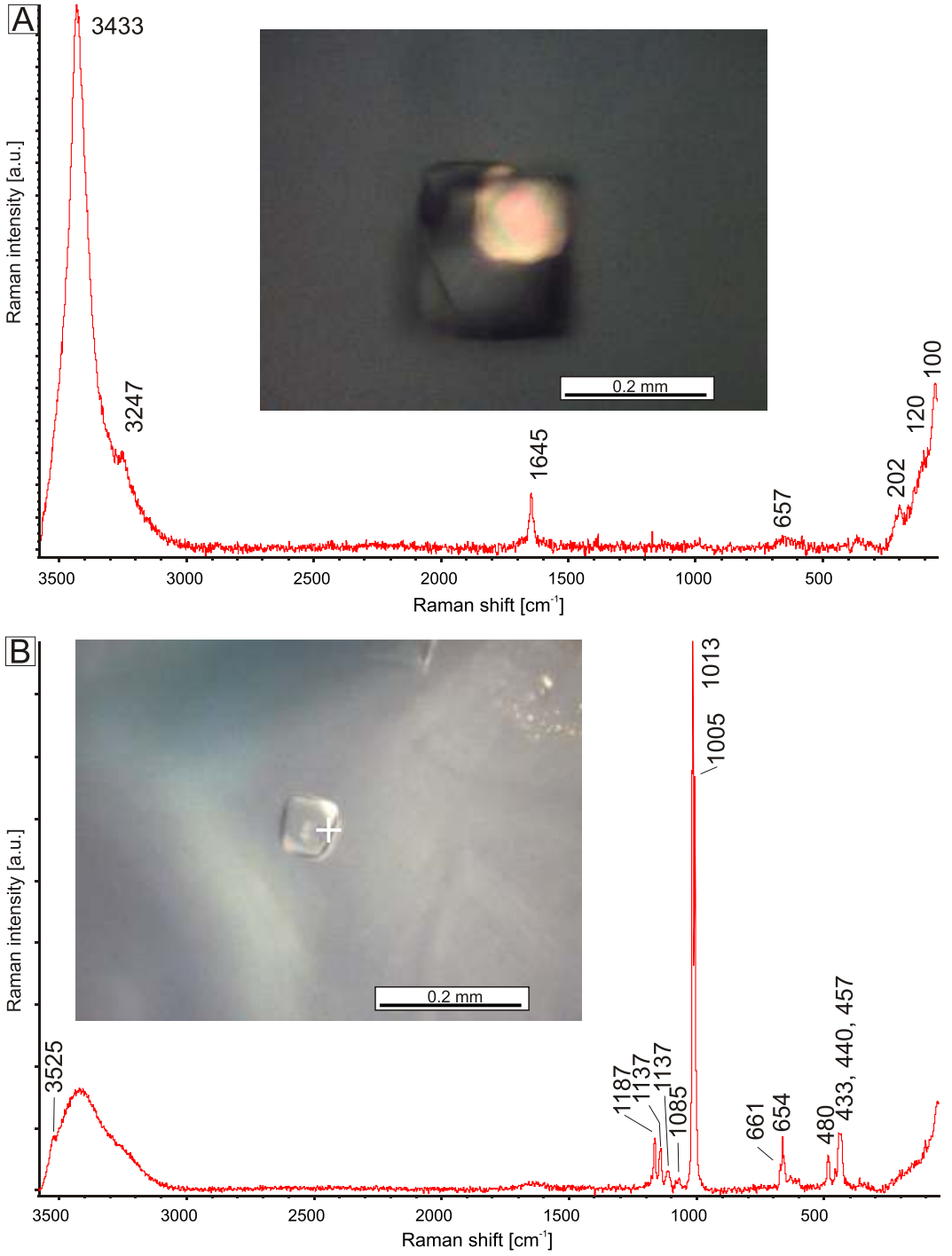

Fig. 8. Raman spectra and microscopic image of: A – fluid inclusion with carnallite daughter mineral (image with partly XN); B – fluid inclusion with görgeyite daughter mineral (image at 1N)

kainite and carnallite or kainite and kieserite, can also result in the release of significant amounts of water (Braitsch, 1971).

A third mechanism to be considered in tectonically deformed salt deposits is associated with halite recrystallization and the expulsion of primary fluid inclusions (Roedder, 1984b; Schléder et al., 2008). Schléder et al. (2008) calculated that ~0.012 m^3 of water is released per 1 m^3 of deformed halite during recrystallization. In the case of LHC veins in the Kłodawa Salt Dome, halite precipitation resulted from a solution that was fully saturated with NaCl. However, fluid inclusion studies indicate that the solution were highly enriched in K and Mg chlorides. This particular chemical composition could not solely result from carnallite decomposition, which forms solutions fully saturated with $MgCl_2$ and KCl; it must also have a low NaCl content. Furthermore, these solutions could not dissolve a significant amount of halite due to the high concentration of chloride ions.

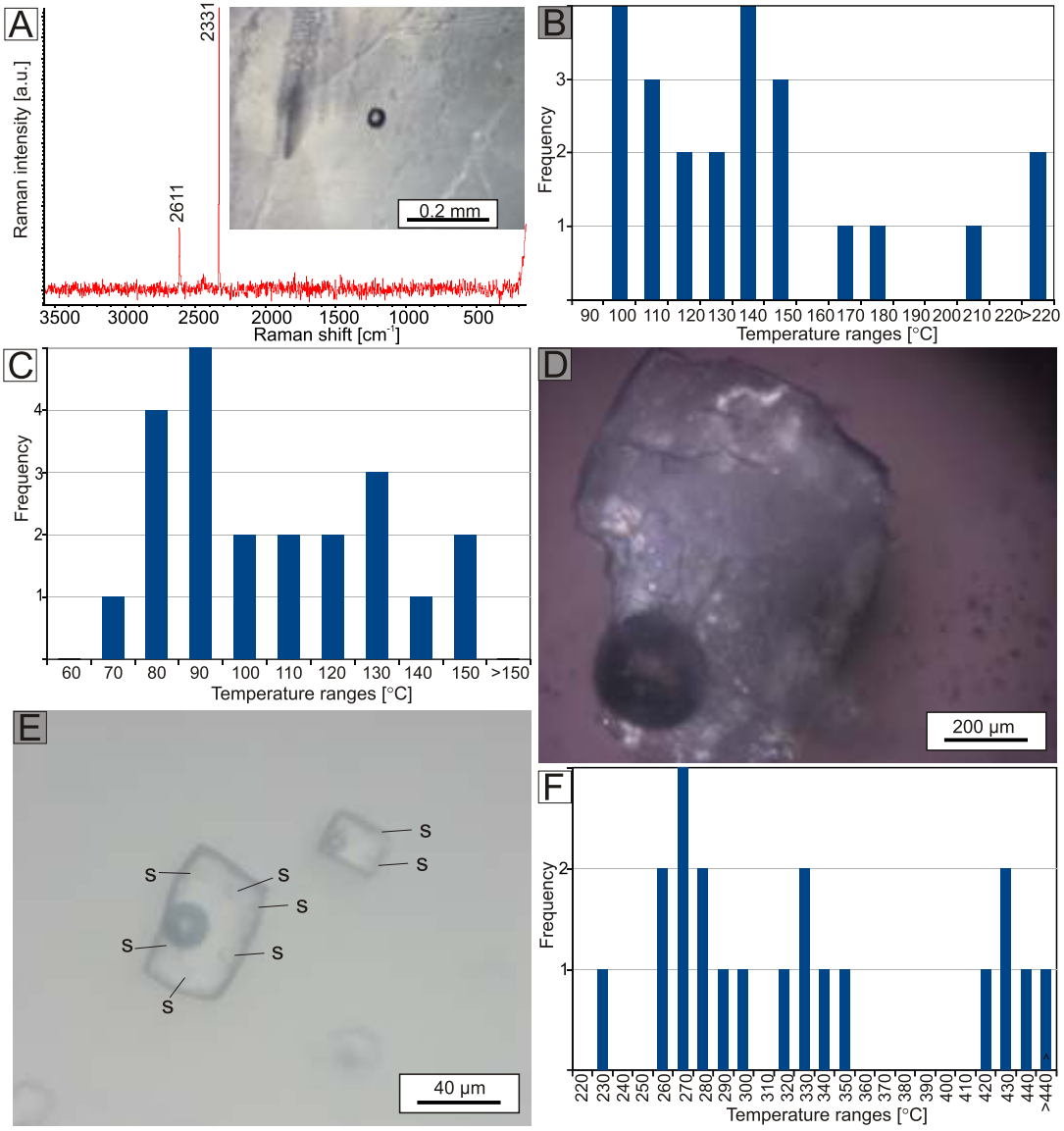

Fig. 9A – Raman spectrum and microscopic image of a single, oval gas (N_2 and H_2S) inclusion; B – histogram of sylvite daughter mineral dissolution temperatures; C – histogram of carnallite daughter mineral dissolution temperatures; D – microscopic image of fluid inclusion with large carnallite daughter mineral after heating and then fast cooling; E – inclusion with sylvite daughter mineral after cooling; F – histogram of the complete homogenization of inclusions

Three forms of anhydrite crystal found in the LHC reflect varying conditions during vein growth and the chemical composition of percolating solutions. The large anhydrite crystals may be regarded as remnants of original sedimentary anhydrite crystals which accompanied primordial halite. Euhedral crystals showing only minor signs of leaching were likely preserved due to the rapid growth of the surrounding LHC, protecting them from the corrosive effects of percolating solutions. These crystals likely represent the initial stage of solution migration during which small amounts of hydrocarbons (bitumen) were transported. The origin of hydrocarbons may relate to the basement of the salt formation (Toboła and Botor, 2020) or the main dolomite (Czechowski et al., 2011; Wagner and Burliga, 2014). The manner in which they occur, specifically in the fracture planes of anhydrite crystals, suggests that fissuring within shear zones was the prevailing process during this initial stage. This fissure propagation allowed solution migration and caused halite recrystallization.

Conversely, the second and third types of anhydrite crystals were exposed to aggressive solutions for extended periods. The third type of anhydrite, consisting of very small crystals arranged in streaks, should be regarded as the youngest, as it formed through crystallization from solutions that migrated within large halite fractures.

Sylvite in the form of oval solid inclusions indicates that this mineral crystallized from solutions earlier than halite in the veins, and then the change in pressure and temperature conditions as well as the chemistry of the solutions caused its partial dissolution and replacement by halite.

Fluid inclusion studies provide the most informative data regarding pressure, temperature, chemical composition of fluids, and fluid migration (Roedder, 1984a; Goldstein and Reynolds,

1994; Goldstein, 2001). Very rare occurrence of primary FIAs in the samples analysed imply a slow growth rate of halite. The presence of carnallite and sylvite daughter minerals indicates that the solutions were highly saturated with K and Mg chloride during the crystallization or recrystallization of LHC. The dissolution temperatures of sylvite daughter minerals in a high range (90.6–278°C) and carnallite daughter minerals in the range 68.1–142°C indicate that the minimum solution temperature during the migration exceeded 70°C. Assuming a thermal gradient of 33°C/km (similar to the present conditions), the depth of LHC crystallization is estimated to be >2 km.

Görgeyite was discovered as a daughter mineral within the fluid inclusions; it is an exceptionally rare sulphate double salt in evaporite deposits and is closely related to syngenite. In evaporite environments, it has been identified in only a few locations. It was first described by Mayrhofer in the Ischler salt deposit (Leopold-Horizon), Salzburg, Austria (Mayrhofer, 1953). It was also found in Lake Inder, Kazakhstan and then in other places such as Greece, Germany and China (Kloprogge et al., 2004). Recently, this mineral was discovered in halite within the Nippawalla Group of Kansas and in the Opeche Shale of North Dakota (Prchlik, 2023). In the Polish part of the Zechstein sedimentary basin, this is the first documented occurrence of this mineral. Görgeyite was also discovered in a geothermal environment in Italy, as reported by Cavarretta et al. (1983). Studies on sulphate synthesis conducted by Kloprogge et al. (2004) suggest a high-temperature (>100°C) genesis for this mineral, which is generally consistent with the temperatures of homogenization of fluid inclusions in halite crystals noted in this study. Moreover, the presence of this mineral in fluid inclusions indicates a high concentration of Ca^{+2} and SO_4^{-2} in the solutions, which is corroborated by the presence of polyhalite in the large halite veins and as a mineral accompanying carnallite in inclusions. Considering the total inclusion homogenization, the temperature of LHC crystallization should be adjusted to higher values and deeper areas of origin. These data should be treated with great caution due to the properties of halite, such as ease of recrystallization, high reactivity with brine, and low mechanical strength. These properties may influence on the obtained homogenization temperatures through shrinkage or swelling of inclusions (Hardie et al., 1983; Roedder 1984a, b). Considering homogenization temperature as the lowest temperature of entrapment of fluid in inclusions, the first range (260–350°C; Fig. 9F and Table 2) would correspond to depths from ~7.9 to ~10.5 km. This range of Zechstein formation burial is slightly larger than the present-day depth, and there are no indications of greater burial of these deposits (Dadlez et al., 1995; Stephenson et al., 2003; Krzywiec, 2004b). The second range (420–471.2°C; Fig. 9F and Table 2) might raise questions due to the high values. These high homogenization temperatures might be explained by the unsealing of inclusions, although no signs of such a process were observed during the petrological observations. Moreover, it should be also taken into account that inclusions which were previously unsealed in the next stage were subject to resealing given the PTV conditions and therefore they represent a high temperature environment. Based on fluid inclusions, the temperature of LHC formation is higher than that resulting from burial of the strata and indicate the input of additional thermal energy, such as via hydrothermal solutions. The influence of hydrothermal solution in the KSD has been discussed in several papers (Wachowiak and Toboła, 2014; Toboła, 2016; Toboła and Wachowiak, 2018; Toboła and Botor, 2020). The most related, in terms of petrological features, to the LHC are blue salts (Toboła et al., 2007; Toboła and Natkaniec-Nowak, 2008; Toboła, 2016). Blue halite usually forms large crystals, but these are distinguished by colour from purple through blue to navy blue and brown. Based on the microthermometric measurements of fluid inclusions in anhydrite crystals included in blue halite crystals, the formation temperature of these rocks was over 250°C (Toboła, 2016). Additional evidence supporting a high temperature influence on the KSD salt rocks was obtained from borate minerals (Wachowiak and Toboła, 2014; Toboła and Wachowiak, 2018). The phase transition and crystal shapes indicate that in some areas of the KSD, temperatures exceeded 339°C.

Considering the petrological and fluid inclusion studies noted above, it can be concluded that the LHC veins and nests formed at elevated temperatures due to the influence of hydrothermal phenomena. The temperatures of their formation should be estimated in the range from 100 to >350°C. The thermal conditions of their formation are similar to those for the formation of blue salts. However, the absence of colour may be attributed to the absence of certain factors, such as reducing conditions (Toboła, 2016). Similar to blue halite, the solutions responsible for LHC crystallization were enriched with ions such as K^+, Mg^{+2}, Ca^{+2}, SO_4^{-2}. This enrichment is likely associated with dissolution of the oldest, older, and younger potassium-magnesium layers. The oldest potassium-magnesium salts have not been discovered in the KSD and other salt domes in Poland up to now. However, they should be expected in the deepest part of the Zechstein basin, as they have been found in its peripheral areas (Peryt and Skowroński, 2021). In the KSD, the older and younger K-Mg salts often exhibit petrological features indicating a substantial degree of transformation (Burliga et al., 1995; Misiek, 1997).

The process of crystallization of relatively large amounts of LHC in the KSD should be associated with a decrease in the temperature of the solutions, because the possibility of evaporation within the salt domes is very limited. During microthermometric measurements, there was no trace of the boiling process that could lead to the release of minerals in the veins (Roedder, 1964b). The solubility of NaCl is dependent on temperature, especially in the range over 100°C (Braitsch, 1971; Bodnar and Vityk, 1994; Bodnar, 2003). Therefore, brines that are fully saturated in NaCl in conditions of higher temperatures will precipitate an excess of NaCl as halite during cooling.

The presence of organic matter (OM) included in LHC may originate from two sources: the Main Dolomite (Ca2) or the Zechstein substrate, as suggested in earlier studies (Toboła and Botor, 2020). Due to the low degree of coalification, the origin of OM from the Main Dolomite (Ca2) is more probable. The temperatures obtained from the distribution of Raman spectra (Table 2) are slightly lower than the homogenization temperatures of the fluid inclusions. This difference can be explained by the short contact time of OM with hydrothermal solutions, not allowing for full carbonization.

CONCLUSIONS

Fluid inclusions and petrological studies of veins and nests of LHC within KSD revealed that:

- this type of salt was formed in shear zones, where the continuity of rock salt layers was broken, which allowed the migration of solutions into the salt dome;
- healing of the veins by LHC took place sometimes under active shear stresses, as shown by the birefringence of halite;
- the veins were formed at elevated temperatures ranging from 100 to over 350°C, which indicates the influence of hydrothermal solutions;

– their crystallization took place from solutions significantly enriched in ions such as K^{+}, Mg^{+2}, Ca^{+2}, SO_4^{-2}, and their source was connected with dissolution of potash-magnesium layers,
– the main process of crystallization of LHC from percolating solutions is associated with a temperature decrease of the mother brines during migration.

Acknowledgements. The author would like to thank M. Weldeghebriel and L. Sahakyan for valuable comments and suggestions which were useful in preparation the final version of this paper. This work was supported by the AGH University of Krakow (16.16.140.315).

REFERENCES

Aoya, M., Kouketsu, Y., Endo, S., Shimizu, H., Mizukami, T., Nakamura, D., 2010. Extending the applicability of the Raman carbonaceous-material geothermometer using data from contact metamorphic rocks. Journal of Metamorphic Geology, **28:** 895–914. https://doi.org/10.1111/j.1525-1314.2010.00896.x

Banaszak, A., Garlicki, A., Markiewicz, A., 2007. Geology of the Oldest Rock Salt Kazimierzów in Sieroszowice I area (Polkowice-Sieroszowice Mine) (in Polish with English summary). Mineral Resources Management, **23**: 9–20.

Beyssac, O., Goffe, B., Chopin, C., Rouzaud, J.N., 2002. Raman spectra of carbonaceous material in metasediments: a new geothermometer. Journal of Metamorphic Geology, **20**: 859–871. https://doi.org/10.1046/j.1525-1314.2002.00408.x

Beyssac, O., Goffe, B., Petitet, J.-P.P., Froigneux, E., Moreau, M., Goffé, B., Petitet, J.P.P., Froigneux, E., Moreau, M., Rouzaud, J.N., 2003. On the characterization of disordered and heterogeneous carbonaceous materials by Raman spectroscopy. Spectrochimica Acta – Part A: Molecular and Biomolecular Spectroscopy, **59**: 2267–2276. https://doi.org/10.1016/S1386-1425(03)00070-2.

Beyssac, O., Bollinger, L., Avouac, J.P., Goffe, B., Goffé, B., 2004. Thermal metamorphism in the Lesser Himalaya of Nepal determined from Raman spectroscopy of carbonaceous material. Earth and Planetary Science Letters, **225**: 233–241. https://doi.org/10.1016/j.epsl.2004.05.023 .

Bodnar, R.J., 2003. Interpretation of data from aqueous-electrolyte fluid inclusions. Mineralogical Association of Canada, Short Course Series, **32**: 81–100.

Bodnar, R.J., Vityk, M.O., 1994. Interpretation of microthermometric data for H_2O-NaCl fluid inclusions. In: Fluid Inclusions in Minerals, Methods and Applications (eds. B. De Vivo and M.L. Frezzotti): 117–130. Virginia Tech, Blacksburg, VA.

Borchert, H., Muir, R.O., 1964. Salt Deposits. The Origin, Metamorphism and Deformation of Evaporites. D. Van Nostrand Company, LTD, Londyn.

Braitsch, Q., 1971. Salt Deposits Their Origin and Compostion. Springer, Berlin.

Burke, E.A.J., 2001. Raman microspectrometry of fluid inclusions. Lithos, **55**: 139–158. https://doi.org/10.1016/S0024-4937(00)00043-8

Burliga, S., Kolonko, P., Misiek, G., Czapowski, G., 1995. Kłodawa salt mine. Upper Permian (Zechstein) profile from basin center, salt tectonics, mineral transformations, salt mining problems. XIII International Congress on Carboniferous-Permian. Guide to Excursion A3: 45–54.

Carter, N.L., Heard, H.C., 1970. Temperature and rate dependent deformation of halite. American Journal of Science, **269:** 193–249.

Cavarretta, G., Mottana, A., Tecce, F., 1983. Görgeyite and syngenite in the Cesano geothermal field (Latium, Italy). Neues Jahrbuch für Mineralogie Abhandlungen, **147**: 304–314.

Cheng, H., Li, J., Hai, Q., Song, J., Ma, X., 2019. Raman and XRD study of polyhalite ore during calcinations. Vibrational Spectroscopy, **102**: 63–70. https://doi.org/10.1016/j.vibspec.2019.04.007.

Cyran, K., Toboła, T., Kamiński, P., 2023. Experimental study on mechanically driven migration of fluids in rock salt. Engineering Geology, **313**: 106975. https://doi.org/10.1016/j.enggeo.2022.106975.

Czapowski, G., Tomassi-Morawiec, H., Tadych, J., Grzybowski, Ł., Sztyrak, T., 2009. Characteristics and tectonics of Zechstein salt rocks of the Góra salt diapir near Inowrocław on the basis of geochemical-lithological study of selected borehole sections (in Polish with English summary). Przegląd Geologiczny, **57:** 494–503.

Czechowski, F., Burliga, S., Hojniak, M., 2011. Geochemistry of hydrocarbons from the first time documented occurrence of Main Dolomite (Ca2) in the Kłodawa Salt Dome (in Polish with English summary). Geologia Kwartalnik AGH, **37**: 231–244.

Dadlez, R., 2003. Mesozoic thickness pattern in the Mid-Polish Trough. Geological Quarterly, **47** (3): 223–240.

Dadlez, R., Narkiewicz, M., Stephenson, R.A., Visser, M.T.M., van Wees, J.D., 1995. Tectonic evolution of the Mid-Polish Trough: modelling implications and significance for central European geology. Tectonophysics, **252**: 179–195. https://doi.org/10.1016/0040-1951(95)00104-2

Frezzotti, M.L., Tecce, F., Casagli, A., 2012. Raman spectroscopy for fluid inclusion analysis. Journal of Geochemical Exploration, **112**: 1–20. https://doi.org/10.1016/j.gexplo.2011.09.009

Galamay, A.R., Meng, F., Bukowski, K., Lyubchak, A., Zhang, Y., Ni, P., 2019. Calculation of salt basin depth using fluid inclusions in halite from the ordovician ordos basin in China. Geological Quarterly, **63** (3)**:** 619–628. https://doi.org/10.7306/gq.1490

Garlicki, A., Szybist, A., 1986. Saline deposits of Polish Zechstein with potash salts (in Polish with English summary). Mineral Resources Management, **2**: 389–404.

Garlicki, A., Szybist, A., 1991. Pierwiastki śladowe w solach kopalni kłodawskiej (in Polish). Prace Specjalne PTMin, **1**: 71–76.

Garlicki, A., Szybist A., 2008. Geological structure of Kłodawa Salt Dome (in Polish with English Summary). In: Blue Halite of the Kłodawa Salt Dome (eds. T. Toboła and L. Natkaniec-Nowak): 13–23. AGH University of Science and Technology Press, Kraków.

Goldstein, R.H., 2001. Fluid inclusions in sedimentary and diagenetic systems. Lithos, **55:** 159–193. https://doi.org/10.1016/S0024-4937(00)00044-X

Goldstein, R.H., 2003. Petrographic analysis of fluid inclusions. Mineralogical Association of Canada, Ottawa.

Goldstein, R.H., Reynolds, J.T., 1994. Systematics of fluid inclusions in diagenetic minerals. SEPM Short Course, **31**: 1–199.

Hardie, L.A., Lowenstein, T.K., Spencer, R.J., 1983. The problem of distinguishing between primary and secondary features in evaporites. In: Sixth International Symposium on Salt (eds B.C. Schreiber and C. Harner): Salt Institute, Alexandria, 1: 11–39.

Heflik, W., Natkaniec-Nowak, L., Toboła, T., 2008. Microscopic investigation of blue salts (in Polish with English summary). Blue Halite of the Kłodawa Salt Dome (eds. T. Toboła and L. Natkaniec-Nowak): 56–69. AGH University of Science and Technology Press, Kraków.

Holdoway, K.A., 1973. Behavior of fluid inclusions in Salt During Heating and Irradiation. Fourth Symposium on Salt April 8–12 (ed. A.H. Coogan): 303–312. Northern Ohio Geological Society, Cleveland.

Jentzsch, P.V., Bolanz, V.B., Ciobotă, V., Kampe, B., Rösch, P., Majzlan, J., Popp, J., 2012. Raman spectroscopic study of calcium mixed salts of atmospheric importance. Vibrational Spectroscopy, **61**: 206–13. https://doi.org/10.1016/j.vibspec.2012.03.007**.**

Kloprogge, J.T., Hickey, L., Duong, L.V., Martens, W.N., Frost, R.L., 2004. Synthesis and characterization of $K_2Ca_5(SO_4)_6{\cdot}H_2O$, the equivalent of görgeyite, a rare evaporite mineral. American Mineralogist, **89**: 266–272. https://doi.org/10.2138/am-2004-2-302.

Kouketsu, Y., Mizukami, T., Mori, H., Endo, S., Aoya, M., Hara, H., Nakamura, D., Wallis, S., 2014. A new approach to develop the Raman carbonaceous material geothermometer for low-grade metamorphism using peak width. Island Arc, **23**: 33–50. https://doi.org/10.1111/iar.12057

Kovalevich, V.M., Jarmołowicz-Szulc, K., Peryt, T.M., Poberegski, A.V., 1997. Messinian chevron halite from the Red Sea (DSDP sites 225 and 227): fluid inclusion study. Neues Jahrbuch für Mineralogie Monatshefte, (10): 433–450. https://doi.org/10.1127/njmm/1997/1997/433.

Koyi, H.A., 1998. The shaping of salt diapirs. Journal of Structural Geology, **20**: 321–338. https://doi.org/10.1016/S0191-8141(97)00092-8

Krantz, M., Luty, F., 1985. Electric-field-induced first-order Raman scattering in pure KCl and KBr. Physical Review B, **31**: 2599–2601. https://doi.org/10.1103/PhysRevB.31.2599

Krzywiec, P., 2004a. Basement vs. salt tectonics and salt-sediment interaction – case study of the Mesozoic Evolution of the Intracontinental Mid-Polish Trough. GCSSEPM Foundation 24th Annual Research Conference "Salt-Sediment Interactions and Hydrocarbon Prospectivity: Concepts, Applications and Case Studies for the 21st Century": 343–370.

Krzywiec, P., 2004b. Triassic evolution of the Kłodawa salt structure: basement-controlled salt tectonics within the Mid-Polish Trough (Central Poland). Geological Quarterly, **48** (2): 123–134.

Krzywiec, P., 2006. Structural inversion of the Pomeranian and Kuiavian segments of the Mid-Polish Trough – lateral variations in timing and structural style. Geological Quarterly, **50** (1): 151–167.

Krzywiec, P., Kramarska, R., Zientara, P., 2003. Strike-slip tectonics within the SW Baltic Sea and its relationship to the inversion of the Mid-Polish Trough – evidence from high-resolution seismic data. Tectonophysics, **373**: 93–105. https://doi.org/10.1016/S0040-1951(03)00286-5

Kucia, Z., 1970. New stratigraphical links of the Zechstein in salt mine "Kłodawa" (in Polish with English summary). Przegląd Geologiczny, **18**: 345–346.

Kupfer, D.H., 1976. Shear zones inside Gulf Coast salt stocks help to delineate spines of movement. AAPG Bulletin, **60**: 1434–1447. https://doi.org/10.1306/C1EA387A-16C9-11D7-8645000102C1865D

Kupfer, D.H., 1980. Problems associated with anomalous zones in Louisiana salt stocks, USA. Fifth Symposium on Salt – Hamburg, Germany, June 1978: 1 (eds. A.H. Coogan and H. Lukas): 119–134. Northern Ohio Geological Society, Cleveland OH.

Kupfer, D.H., 1990. Anomalous features in the five islands salt stocks, Louisiana. Gulf Coast Association of Geological Societies Transactions, **40**: 425–437.

Lahfid, A. Beyssac, O., Deville, E., Negro, F., Chopin, C., Goffe, B., Goffé, B., 2010. Evolution of the Raman spectrum of carbonaceous material in low-grade metasediments of the Glarus Alps (Switzerland). Terra Nova, **22**: 354–360. https://doi.org/10.1111/j.1365-3121.2010.00956.x

Looff, K., 2017. The Impact of Anomalous Salt and Boundary Shear Zones on Salt Cavern Geometry, Cavern Operations, and Cavern Integrity. In: Proceedings of the American Gas Association, Operating Section, 2017–May: 267–96.

Looff, K.M., Looff, K.M., Rautman, C., 2010. Inferring the geologic significance and potential impact of salt fabric and anomalous salt on the development and long-term operation of salt storage caverns on Gulf Coast Salt Domes. SMRI Spring 2010 Technical Conference 26–27 April 2010 Grand Junction, Colorado, USA.

Lünsdorf, N.K., 2016. Raman spectroscopy of dispersed vitrinite – methodical aspects and correlation with reflectance. International Journal of Coal Geology **153**: 75–86. https://doi.org/10.1016/j.coal.2015.11.010

Lünsdorf, N.K., Lünsdorf, J.O., 2016. Evaluating Raman spectra of carbonaceous matter by automated, iterative curve-fitting. International Journal of Coal Geology, **160–161**: 51–62. https://doi.org/10.1016/j.coal.2016.04.008

Lünsdorf, N.K., Dunkl, I., Schmidt, B.C., Rantitsch, G., von Eynatten, H., 2013. Towards a higher comparability of geothermometric data obtained by Raman spectroscopy of carbonaceous material. Part I: Evaluation of biasing factors. Geostandards and Geoanalytical Research, **38**: 73–94. https://doi.org/10.1111/j.1751-908X.2013.12011.x

Łaszkiewicz, A., 1967. Salt minerals and rocks (in Polish with English summary). Prace Muzeum Ziemi, **11:** 100–188.

Mayrhofer, H., 1953. Gorgeyit. Ein neues Mineral aus der Ischler Salzlagerstatte. Neues Jahrbuch für Mineralogie Monatshefte, (2): 35–44.

Mendelson, S., 1961. Birefringence due to dislocations in glide bands of rocksalt single crystals. Journal of Applied Physics, **32**: 1999–2004. https://doi.org/10.1063/1.1728278

Misiek, G., 1997. Stratygrafia i wykształcenie utworów cechsztynu w wysadzie solnym Kłodawy (in Polish). Conference Materials on Salt Tectonics of the Kujawy Region, Uniejów (ed. S. Burliga): 20–23. 23–25.10.1997. Uniejów: WIND: Wrocław, Poland.

Peryt, T.M., Skowroński, L., 2021. The stratigraphy of Zechstein strata in the East European Craton of Poland: An overview. Geological Quarterly, **65**: 48. https://doi.org/10.7306/gq.1617

Prchlik, R.J., 2023. A study of accidental daughter crystals in fluid inclusions in bedded halite from the Permian Opeche Shale and Cedar Hills Sandstone of the midcontinental United States. M.Sc. Thesis, West Virginia University.

Roedder, E., 1984a. Fluid inclusions. Reviews in Mineralogy, **12**: 1–646.

Roedder, E., 1984b. The fluids in salt. American Mineralogist, **69**: 413–439.

Schléder, Z., Burliga, S., Urai, J.L., 2007. Dynamic and static recrystallization-related microstructures in halite samples from the Kłodawa salt wall (central Poland) as revealed by gamma-irradiation. Neues Jahrbuch für Mineralogie Abhandlungen, **184**: 17–28. https://doi.org/10.1127/0077-7757/2007/0079

Schléder, Z., Urai, J.L., Nollet, S., Hilgers, C., 2008. Solution-precipitation creep and fluid flow in halite: a case study of Zechstein (Z1) rocksalt from Neuhof salt mine (Germany). International Journal of Earth Sciences, **97:** 1045–1056. https://doi.org/10.1007/s00531-007-0275-y

Sonnenfeld, P., 1984. Brines and Evaporites. Academic Press, Inc., Orlando, Fla.

Sonnenfeld, P., 1995. The color of rock salt – a review. Sedimentary Geology, **94**: 267–276. https://doi.org/10.1016/0037-0738(94)00093-A

Stańczyk, I., 1970. Polyhalite in the salt mines of the Kujawy region (in Polish with English summary). Acta Geologica Polonica, **20:** 805–821.

Stańczyk-Stasik I., 1976. Les dépots épigénétiques dans les mines de sel de la région de Kujawy (in Polish with French summary). Prace Geologiczne, **90**: 1–64.

Stephenson, R.A. Narkiewicz, M., Dadlez, R., Diederik van Wees, J., Andriessen, P., 2003. Tectonic subsidence modelling of the Polish Basin in the light of new data on crustal structure and magnitude of inversion. Sedimentary Geology, **156**: 59–70. https://doi.org/10.1016/S0037-0738(02)00282-8

Talbot, C.J., 1993. Spreading of salt structures in the Gulf of Mexico. Tectonophysics, **228**: 151–166. https://doi.org/10.1016/0040-1951(93)90338-K

Talbot, C.J., Jackson, M.P.A., 1987. Salt tectonics. Scientific Reports, **257**: 70–79.

Toboła, T., 2010. Inclusions in bituminous salts from Kłodawa Salt Dome (in Polish with English summary). Geologia Kwartalnik AGH, **36**: 345–365.

Toboła, T., 2016. Inclusions in anhydrite crystals from blue halite veins in the Kłodawa Salt Dome (Zechstein, Poland). Geological Quarterly, **60** (3): 572–585. https://doi.org/10.7306/gq.1274

Toboła, T., Botor, D., 2020. Raman spectroscopy of organic matter and rare minerals in the Kłodawa Salt Dome (Central Poland) cap-rock and Triassic cover – indicators of hydrothermal solution migration. Spectrochimica Acta – Part A: Molecular and Biomolecular Spectroscopy, **231**, 118121 https://doi.org/10.1016/j.saa.2020.118121

Toboła, T., Kukiałka, P., 2010. The lotsberg salt formation in central Alberta (Canada) – petrology, geochemistry, and fluid inclusions. Minerals, **10.** https://doi.org/10.3390/min10100868

Toboła, T., Natkaniec-Nowak, L., eds., 2008. Sole niebieskie w wysadzie kłodawskim (in Polish). Uczelniane Wydawnictwa Naukowo-Dydaktyczne AGH.

Toboła, T., Wachowiak, J., 2018. Evidence of high-temperature rock salt transformations in areas of occurrence of borate minerals (Zechstein, Kłodawa salt dome, Poland). Geological Quarterly, **62** (1): 134–145. https://doi.org/10.7306/gq.1390

Toboła, T. Natkaniec-Nowak, L., Szybist, A., Misiek, G., Janiów, S., 2007. Blue salts in Kłodawa Salt Mine (in Polish with English summary). Mineral Resources Management, **23:** 117–132.

Trusheim, F., 1960. Mechanism of salt migration in Northern Germany. AAPG Bulletin, **44**: 1519–1540. https://doi.org/10.1306/0BDA61CA-16BD-11D7-8645000102C1865D

Vanko, D.A., Bach, W., 2005. Heating and freezing experiments on aqueous fluid inclusions in anhydrite: recognition and effects of stretching and the low-temperature formation of gypsum. Chemical Geology, **223**: 35–45. https://doi.org/10.1016/j.chemgeo.2004.11.021

Wachowiak, J., 2010. Mineral levels in Upper Permian (Zechstein) salts of the Kłodawa salt diapir as a tool for lithostratigraphic correlation (in Polish with English summary). Geologia Kwartalnik AGH, **36**: 367–393.

Wachowiak, J., Toboła, T., 2014. Phase transitions in the borate minerals from the Kłodawa salt dome (central Poland) as indicators of temperature processes in salt diapirs. Geological Quarterly, **58** (3): 543–554. https://doi.org/10.7306/gq.1170

Wagner, M., Burliga, S., 2014. Coalified bitumens from the Kłodawa Salt Structure (central Poland) as evidence of migration of hydrothermal fluids in Zechstein (Upper Permian) deposits. Geological Quarterly, **58** (3): 555–564. https://doi.org/10.7306/gq.1127

Wagner, R., 1994. Stratigraphy and evolution of the Zechstein Basin in the Polish lowland (in Polish with English summary). Prace Państwowego Instytutu Geologicznego, **146**: 1–71.

Wagner, R., Leszczyński, K., Pokorski, J., Gumulak, K., 2002. Palaeotectonic cross-sections through the Mid-Polish Trough. Geological Quarterly, **46** (3): 293–306.

Wang, A., Freeman, J.J., Jolliff, B.L., Chou, I-M., 2006. Sulfates on Mars: a systematic Raman spectroscopic study of hydration states of magnesium sulfates. Geochimica et Cosmochimica Acta, **70**: 6118–6135 https://doi.org/10.1016/j.gca.2006.05.022

Warren, J.K., 2017. Salt usually seals, but sometimes leaks: Implications for mine and cavern stabilities in the short and long term. Earth-Science Reviews, **165**: 302–341. https://doi.org/10.1016/j.earscirev.2016.11.008

Weber, I., Böttger, U., Pavlov, S.G., Hübers, H.W., Hiesinger, H., 2017. Raman spectra of water bearing minerals at different environmental conditions. Lunar and Planetary Science, **48**: 1–3.

Weber, I., Böttger, U., Pavlov, S.G., Stojic, A., Hübers, H.W., Jessberger, E.K., 2018. Raman spectra of hydrous minerals investigated under various environmental conditions in preparation for planetary space missions. Journal of Raman Spectroscopy, **49**: 1830–1839. https://doi.org/10.1002/jrs.5463

Werner, Z., Poborski, J., Orska, J., Bąkowski, J., 1960. A geological and mining outline of the Kłodawa salt deposit (in Polish with English summary). Prace Instytutu Geologicznego, **30**: 467–512.

Wesełucha-Birczyńska, A., Toboła, T., Natkaniec-Nowak, L., 2008. Raman microscopy of inclusions in blue halites. Vibrational Spectroscopy, **48**: 302–307. https://doi.org/10.1016/j.vibspec.2008.05.005

Wesełucha-Birczyńska, A., Zelek, S., Stadnicka, K., 2012. Vibrational Spectroscopy Blue halite colour centre aggregates studied by micro-Raman spectroscopy and X-ray diffraction. Vibrational Spectroscopy, **60**: 124–128. https://doi.org/10.1016/j.vibspec.2011.11.001

Wojdyr, M., 2010. Fityk: a general-purpose peak fitting program. Journal of Applied Crystallography, **43**: 1126–1128. https://doi.org/10.1107/S0021889810030499

Wollmann, G., Freyer, D., Voigt, W., 2008. Polyhalite and its analogous triple salts. Monatshefte für Chemie, **139**: 739–745.

Wopenka, B., Pasteris, J.D., 1993. Structural characterization of kerogens to granulite-facies graphite: applicability of Raman microprobe spectroscopy. American Mineralogist, **78**: 533–557.

Zelek, S., Stadnicka, K., Szklarzewicz, J., Natkaniec-Nowak, L., 2008. Halite from Kłodawa: the attempt of correlation between lattice deformation and spectroscopic properties in UV-VIS (in Polish with English summary). Mineral Resources Management, **24**: 159–173.

Zelek, S.M., Wesełucha-Birczyńska, A., Szklarzewicz, J., Stadnicka, K.M., 2015. Spectroscopic properties of halite from Kłodawa salt mine, central Poland. Mineralogy and Petrology, **109**: 45–51. https://doi.org/10.1007/s00710-014-0348-0